Electronic Supplementary Material (ESI) for Chemical Communications.

Supporting Information

Extending FRET cascades on linear DNA photonic wires

Christopher M. Spillmann, Susan Buckhout-White, Eunkeu Oh, Ellen R. Goldman, Mario G. Ancona and Igor L. Medintz

DNA design.

The DNA in these experiments were designed synthetic sequences that were purchased from Bio-Synthesis (Lewisville, Tx). The DNA sequences (Table SVIII) were designed such that the inter-dye spacings were proportional to range circa 0.3-to-0.5× the estimated Förster distance (R_0) for each dye pair. To design the DNA structures to assemble the dyes at the appropriate spacings the following formula was used: (Dietrich *et al*., 2002)

(S1) $$R_{DA} = \sqrt{(3.4 * N + K)^2 + \left(L_D^2 + L_A^2 - 2L_D L_A \cos(\phi + 34.3 * N)\right)}$$

where the final spacing is R_{DA}, N is the number of separating bases, K is either 0 or 3.4 depending on whether the dye is on the same DNA helix or the opposite, and L_D and L_A are 1.7, accounting for the 0.7 nm six carbon linker and 1 nm for half the width of the DNA helix. The 34.3 factor comes from the 360° of rotation divided by 10.5, the number of bases in a full turn. This accounts for the linker to which the dye is attached to the DNA, the width of the DNA molecule itself and the radial position around the DNA helix.

Sample assembly and hybridization.

Stock solutions of DNA were diluted into 2.5X PBS at 20 μM working concentration. Individual samples were assembled stepwise from component DNA (20 μM) in 0.5 mL PCR or 1.5 mL Eppendorf tubes to a final concentration of 1 μM in ~110 μLs of 2.5X PBS. $MgCl_2$ was excluded due to the potentially deleterious effects high concentrations of such ions can have on dye fluorescence. The use of high salt concentrations (such as 2.5X PBS) to maintain DNA structures without $MgCl_2$ has been previously validated.{Martin, 2012} Samples were vortexed repeatedly, microcentrifuged, and then placed in a heating block with boiling water in the wells. The block was removed after 1 min and the samples were allowed to cool to ambient temperature for 2 hrs followed by brief microcentrifugation to collect the volume and 1 hr incubation at 4°C. A similar procedure was also used substituting a PCR thermal cycler for the heating block. Replicate structures were assembled for the full constructs and all control permutations thereof with 1 or more dyes missing to estimate other FRET pathways.

Data collection.

Each structure to be tested was typically independently assembled at least in triplicate which usually entailed performing experiments over several days. Assembled structures were aliquoted into microtiter well plates and fluorescence collected on a Tecan Infinite M1000 Dual Monochromator Multifunction Microtiter Plate Reader (Tecan, Research Triangle Park, NC) equipped with a xenon flash lamp using appropriate excitation for the AF488 dye unless otherwise indicated. A 400 Hz flash frequency was used with a 40 μs integration time. Emission spectra were collected from in 1 nm increments and exported into an Excel spreadsheet for later data processing and analysis. The Tecan performs an automatic, calibrated adjustment on collected data for nonlinear detector response in the near-IR, *i.e.* internally corrected.

Estimating energy transfer efficiencies with selected dyes missing in the assembled structures.

Table SI. Estimated area of the deconvolved and direct-excitation corrected terminal AF700 dye in selected constructs with 2 dyes missing.

Construct	PL Area ($\times 10^4$)
x - x - Cy3.5 - AF610 - Cy5 - Cy5.5 - AF700	1.96
Fl - x - x - AF610 - Cy5 - Cy5.5 - AF700	2.38
Fl - Cy3 - x - x - Cy5 - Cy5.5 - AF700	2.68
Fl - Cy3 - Cy3.5 - x - x - Cy5.5 - AF700	4.72
Fl - Cy3 - Cy3.5 - AF610 - x - x - AF700	2.54

Table SII. FRET and *E* for selected longer range interactions

Construct	Donor Emission Loss	Sensitized Acceptor Emission*	*E*
Fl - x - Cy3.5	60.9 %	14.9 %	41.5 %
Cy3 - x - x - Cy5	15.5 %	15.0 %	17.5 %
Cy3.5 - x - Cy5	24.5 %	32.5 %	37.1 %

*Determined as described in Spillmann et al, 2013.

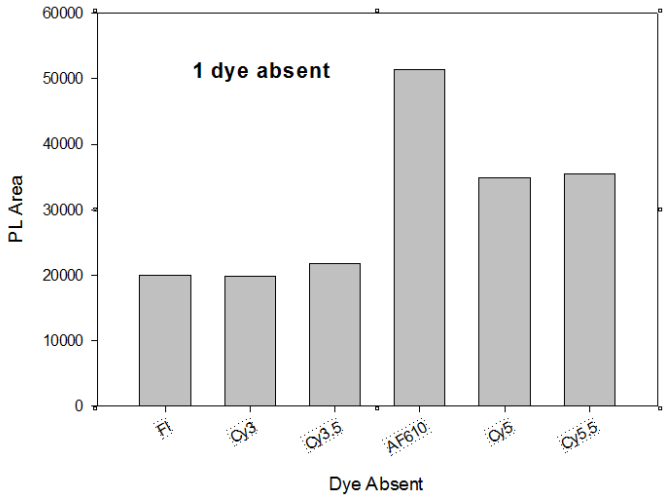

Figure S1. Estimated areas of the deconvolved and direct-excitation corrected terminal AF700 dye in selected constructs with 1 dye missing.

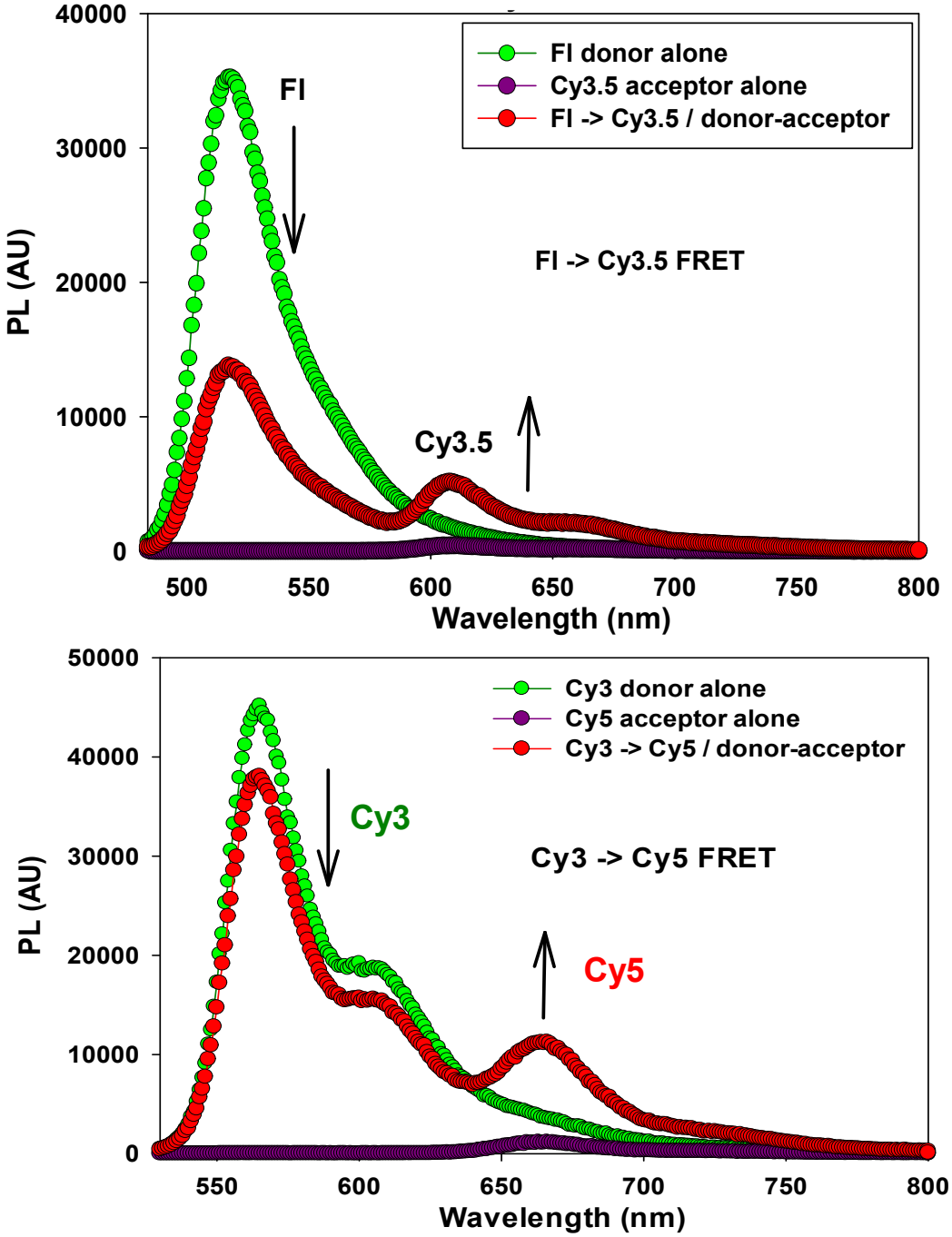

Figure S2. Representative spectra collected from assemblies containing only the indicated donor-acceptor dyes to estimate the potential for longer range energy transfer and end-to-end efficiencies *E* through the system.

The table, graphs and data shown above report the PL area of terminal dye AlexaFluor700 (AF700) in various constructs with one or two dyes missing along with interrogating constructs that only have 2 dyes present to isolate their interactions and estimate the potential for long range energy transfer and the associated end-to-end efficiency. These data are also insightful for identifying which fluorophores are most effective acting as FRET relays to downstream fluorophores and, in a similar vein, which dyes are most critical in optimizing throughout across this 7-dye, 6-FRET step photonic wire. Removing upstream fluorophores, such as fluorescein and Cy3, results in the lowest PL of AF700. Since these dyes, and particularly fluorescein, have the largest direct excitation, they also offer the best potential output to adjacent dyes within the Förster regime (given the photophysical parameters of each particular dye). Conversely, removal of these components places the most severe limits on the energy *available* for transfer. The performance of the photonic wire is largely unaffected by the removal of downstream dyes (Cy5 and Cy5.5), presumably due to the effectiveness of the photonic wire design (spacing and dye selection) to accommodate missing transfer steps.

A significant increase in the PL area of AF700 is observed when two intermediate dyes, AF610 and Cy5 are removed from the wire. This follows a similar trend observed in the absence of only AF610 from the photonic wire. This indicates one or both of these dyes are not acting ideally as effective relays along the photonic wire. Supporting this, it is noteworthy that the end-to-end efficiency determined E in the Fl-Cy3-Cy3.5-AF610 construct (2.6 ± 0.3%) has a sharp drop from the value of the Fl-Cy3-Cy3.5 construct (80 ± 20%) that is not expected given the spacing and spectral overlap between Cy3.5 and AF610. In addition, these data also indicate the remaining dyes present on the wire more than compensate for the poor relay of energy through a single step of the transfer process, resulting in an increase in the PL area of the terminal dye, AF700. By designing the photonic wires with a series of dyes with close spacings ($\leq 0.5 \times R_0$), significant spectral overlap, and some with a broad absorption spectrum, we have demonstrated an effective photonic wire with sufficient redundancy to compensate for poor performance of a single or more dye component This further elucidates the design rules for effective energy transfer through multiple steps and over a large portion of the visible and near-infrared spectrum.

Analysis Approach.

The goal of the analysis is to understand the measured photoluminescence spectra that characterize the photonic wires being studied in a manner similar to that used for Spillmann *et al*., 2013. For any given sample (under particular conditions of concentration, illumination, etc.), the PL spectrum $G(\lambda)$ provides the number of emitted photons collected per unit wavelength per second into the detector. Because the emission of the different dyes are well separated in wavelength, the composite spectrum $G(\lambda)$ is readily decomposed into individual contributions and the integrals of these component spectra, denoted by Φ_i, give the total emission from each dye. The spectral decomposition is thus:

$$G(\lambda) = \sum_{i=1}^{N} f_i(\lambda)\Phi_i \qquad and \qquad G_i^0(\lambda) = f_i(\lambda)\Phi_i^0 \tag{1}$$

(S2)

where $N \leq 7$ is the number of dyes in the particular wire and $f_i(\lambda)$ is the normalized emission spectrum of dye i. The second expression in (S2) is the direct excitation spectrum obtained when only a single type of dye is present.

For the analysis of the photonic wire spectra we employ Förster theory. This approach is likely adequate, however, a chief obstacle to reaching an unambiguous understanding is the potentially large number of parameters such a model can contain that can very easily allow excellent curve-fits to data to be obtained while offering little or no physical insight. Consequently, we look to create a simple but sensible model, whose parsimony prevents exact curve fitting of the entire data set, and whose physical fidelity can be assessed by comparing its predictions with experiment.

To develop the "simple" model, we suggest that the relative simplicity of the photonic wires make it likely the measured samples will be relatively homogeneous with few partial structures or unhybridized dyes. Moreover, since the wires use a single DNA duplex of moderate length as a scaffold, it seems reasonable to suppose that the wires will remain straight/rigid under all circumstances. We therefore assume the experimental samples consist of *uniform* ensembles of structures. In doing so, we surrender any ability to treat the randomness of the flexible linkers that tie the dyes to the DNA scaffold, and our model thus incorporates only "average" dye positions. A final simplifying assertion of our model is that we assume consistency between

different wire configurations, meaning that over the entire data set all aspects of the dyes including their positions and quantum yields are taken to remain unchanged.

The analysis is based on a set of coupled rate equations that describe the various energy transfer processes that can occur within the photonic wires. When normalized by total concentration the variables in these equations become probabilities, and for the "homogeneous" photonic wire model, the governing equations may be written as

$$\frac{dP_i}{dt} = \alpha_i \eta_i \delta(t) - \frac{P_i}{\tau_i}\left[1 + \sum_{j=i+1}^{N} \alpha_j b_{ij}\right] + \alpha_i \sum_{j=1}^{i-1} \frac{b_{ji} P_j}{\tau_j} \qquad i = 1,\ldots,N \tag{S3}$$

where $P_i(t)$ is the probability that dye *i* will be excited at time *t*, τ_i is the lifetime of dye *i*, α_i is its probability of being present/active, the matrix b_{ij} specifies the excitonic coupling between dyes *i* and *j*, and the term containing the δ-function models the direct excitation as derived from single-dye control experiments (see below). We assume the dye couplings are described by Förster theory in which case

$$b_{ij} = \left(\frac{R_0^{ij}}{r_{ij}}\right)^6 \qquad r_{ij} \cong \sum_{k=i}^{j-1} r_{k,k+1} \tag{S4}$$

where R_0^{ij} is the Förster distance characterizing the strength of the coupling between a donor dye of type *i* and an acceptor dye of type *j*, and r_{ij} is the distance between these dyes. The approximation on the right reflects the linearity of the wire and the idea that non-nearest neighbor distances can be approximated as sums of the nearest neighbor distances.

Since the emission rate from dye *i* is given by $Q_i P_i/\tau_i$ where Q_i is the dye's quantum yield, the total number of photons emitted (per photon absorbed) by dye *i* will be $Q_i W_i$ where

$$W_i \equiv \frac{1}{\tau_i}\int_0^\infty P_i(t)\, dt \tag{S5}$$

Equations governing the W_i are readily obtained by integrating (S3) over time (and using the fact that no dyes are excited prior to the initial excitation or remain excited after infinite time) to find:

$$W_i\left[1 + \sum_{j=i+1}^{N} \alpha_j b_{ij}\right] - \alpha_i \sum_{j=i}^{i-1} b_{ji} W_j = \alpha_i \eta_i, \qquad i = 1, \ldots, N \tag{S6}$$

(S6)

which is a system of N linear algebraic equations in N unknowns. Lastly, to connect with experiment we need to relate the quantities in (S6) to the PL areas Φ_i of $(S2)_1$ that represent the total emitted energy into the detector per second by dyes of type i. Specifically, we have

$$\Phi_i = \Psi Q_i W_i \qquad i = 1, \ldots, N \tag{6}$$

(S7)

where $\Psi \equiv \rho A L \Omega$ is a scaled generation rate (where ρ is the concentration, A is the number of photons absorbed per second by a single structure, L is the path length, and Ω is a geometric factor expressing the fraction of emitted photons that make it to the detector). Based on single-dye control experiments (in which the concentrations are presumed the same and $\alpha_i = 1$) and $(S2)_1$ and (S6), one has $\Phi_i^0 = \Psi Q_i \eta_i$ and it then follows that

$$\eta_i = \frac{\Phi_i^0}{\Psi Q_i} \qquad \Psi = \sum_{i=1}^{N} \frac{\Phi_i^0}{Q_i} \tag{7}$$

(S8)

The second equality in (7) provides a way of estimating the normalization, and since to the extent possible all is kept fixed in the experiments (concentrations, illumination, etc.), just one value of Ψ can suffice for all experiments.

If the forgoing is to provide a consistent description of a given set of photonic wire experiments, we need to be able to select the "unknowns" of the description so that the simulated PL spectra are in good agreement. To this end, we take the fitting parameters of the model to be the 6 nearest neighbor distances $r_{k,k+1}$, the 7 α_i and the 7 ΨQ_i values (with Ψ merged with Q_i since they always appear as a product) for a total of 20 parameters. Again, that the same parameter values should apply in different experiments is a basic assertion of our approach; assessing whether or not this is justified must come *a posteriori* from the quality of the results. Note also that treating both α_i and Q_i as fitting parameters means that the model is allowing non-ideal dye performance to result both from the dyes being partially absent/inactive and by them having reduced radiative efficiency (i.e., acting as a strong quencher). Such effects are possible because the dyes, while all functioning well by themselves in control experiments, occur in the photonic wires in very close proximity to other dyes. Phenomena such as photobleaching could also play

a role. The justification for not having the R_0^{ij} be fitting parameters is that they occur only in ratio with r_{ij} and so are largely represented by $r_{k,k+1}$. Hence we simply assume the R_0^{ij} take their "ideal" values (as estimated from a standard Förster theory, see Table SVIII), keeping in mind that when interpreting the $r_{k,k+1}$ values obtained from curve-fitting, one possibility is that they are representing the influence of "non-ideal" R_0^{ij}'s. The values of η_m and Ψ are estimated from control experiments using (S8) with Ψ found to be $\Psi_{scal} \equiv 3.5x10^6$ and the η_m are as given in Table SIIIa.

In essence, we use this 20-parameter model to fit experimental values for the Φ_i, in particular, using data from six (M = 6) experiments in which dyes are progressively added to the wire with N = 2, 3, 4, 5, 6, and 7. This implies that there are 2+3+4+5+6+7 = 27 different experimental numbers that are being fit. To do the fitting we employ standard least-square regression in which the error is minimized.

$$\varepsilon = \sum_{m=1}^{M} \sum_{i=1}^{N_m} \left[\left(\Phi_i^m\right)^{exp} - \left(\Phi_i^m\right)^{sim} \right]^2 \qquad \text{(S9)} \quad (8)$$

To this expression one could also add penalty terms to enforce certain limits on the unknowns, e.g., $r_{k,k+1} > 0$ or $0 \le \alpha_i \le 1$, but this was found to be unnecessary. A more serious complication is the fact that the regression error surface defined by (S9) is found to have local minima and so we vary the initial guesses and search for the global minimum. To give a sense of scale for the various parameters, the "ideal" values for Q_i listed in Table SVIII, the parameters α_i are ideally unity, and a lower bound on the nearest-neighbor dye spacings $r_{k,k+1}$ can be found from the distances between the dye attachment points on the DNA scaffold. Approximate values for these spacings can be obtained from the cylinder model of (S1) with L_D and L_A set to 1 nm and are given in Table SIIIb.

Simulation Results

Carrying out the numerical regression as described in the previous section, we obtain the fits shown in Fig. S4 to the 6 experiments with progressively increasing numbers of dyes in the wire. Overall the fits seem quite good, with the biggest discrepancy being for the two-dye (Fl and Cy3) case where the Fl emission is significantly underestimated. The values of the 20 parameters required to obtain these fits are listed in Table SIV, and from an examination of them three observations seem most noteworthy. First, the nearest-neighbor dye distances $R_{k,k+1}$ are quite reasonable. To see this, we list also in Table SIV the differences ($\Delta R_{k,k+1}$) between the $R_{k,k+1}$ values obtained from the fitting and the dye attachment point distances. Given their size (always less than 25Å), it seems reasonable to suggest that these "excess" distances can result entirely from the two linkers involved, the size of the two dye molecules, and the overall geometry (although as noted earlier they might also account for non-ideality in the R_0^{ij}). More concretely, in Fig. S3 we show a crude depiction of the wire with all of the dyes taken to be oriented radially (on average). The positioning of the dyes is meant to reflect which strand the dyes are on and the effect of the helicity, e.g., A610 and Cy5 are depicted on the same side of the DNA since they are on the same strand and separated by 10 bp (as indicated in blue in the figure) or one full helical turn. Also shown in the figure are the $\Delta R_{k,k+1}$ values and these are seen to correspond somewhat with the schematic. Most interesting is that the value for the A610-Cy5 pair (ΔR_{45}) is zero, and this is as "expected" given that these dyes are the only nearest-neighbor pair that is perfectly lined up on the same side of the helix. Why the other numbers take the values they do is less clear, but certainly not unreasonable. The second observation regarding Table SIV is that the values of $\Psi Q_i/\Psi_{scal}$ are in fair agreement with the "ideal" Q_i values listed in Table SVIII with no deviations so large as to not be plausible. Finally, the "yield" values obtained for the α_i (Table SIV) are also mostly relatively close to one, with the outstanding exception being that of A610 which is instead quite close to zero ($\alpha_4 \cong 1.3\%$). This immediately suggests that the observed poor performance of the extended wire is due to the A610 dye mostly being absent/inactive.

In general, the foregoing discussion of the model parameters in Table SIV as derived from the regression in Fig. S5 form a plausible interpretation of the photonic wire configuration (Fig. S3) and its behavior. Given this, we proceed with a further test of the model in which we make predictions of the spectra for other wire configurations and compare these with measurements.

The particular experiments used for this validation have the photonic wire with its full complement of dyes except for one dye missing. The experimental spectra and the corresponding simulations (all made with the parameter set of Table SIV) are shown in Fig. S4 with the labels indicating the missing dye in each experiment. In most cases the experiments are found to be predicted quite accurately by the model, with the biggest disagreement being for the Fl emission from the wire missing the Cy3 dye. Another way of viewing these results is to compare the predicted anywhere-to-end efficiencies with the experimental results shown in Manuscript Fig. 4D. The analogous plot of the predicted efficiencies appear in Fig. S5 (labeled "actual") and good agreement is again seen, including that the prediction also exhibits the curious rise in efficiency when the A610 dye is omitted.

The general plausibility of the regression-determined model parameters, plus the overall agreement seen in the missing-dye experiments between model prediction and experimental measurement support the idea that our physical model as embodied in Fig. S3 does indeed have some validity. On this basis, a major conclusion of the analysis is that the extended photonic wire performs poorly because the A610 dye is mostly absent/inactive and that further work in this area should look to improve the A610 performance. How much can be expected from instituting such improvements is readily addressed with simulation. In Fig. S5 we show not only the predicted "actual" efficiencies of the missing-dye wires, but also simulated "ideal" efficiencies, with values shown with just the contribution of an ideal α_i (i.e., $\alpha_i = 1$) and when Q_i is also given ideal values (Table SVIII). As seen in Fig. S5, these changes result in the anywhere-to-end efficiencies showing substantial improvements. In the case of the photonic wire with all 7 dyes, the anywhere-to-end efficiency is about 5.7% in the actual situation, this improves to 17.4% when $\alpha_i = 1$, and rises further to 26.2% when Q_i is also made ideal.

Supporting References:

C.M. Spillmann, M.G. Ancona, S. Buckhout-White, W.R. Algar, M. H. Stewart, K. Susumu, A.L. Huston, E.R. Goldman, and I.L. Medintz, Achieving Effective Terminal Exciton Delivery in Quantum Dot Antenna-Sensitized Multistep DNA Photonic Wires, *ACS Nano*, 2013, **7**, 7101.

A. Dietrich, V. Buschmann, C. Muller, M. Sauer, Fluorescence resonance energy transfer (FRET) and competing processes in donor-acceptor substituted DNA strands: a comparative study of ensemble and single-molecule data, *Reviews in Molecular Biotechnology,* 2002, **82**, 211.

Martin, T. G. and H. Dietza (2012). "Magnesium-free self-assembly of multi-layer DNA objects." Nature Communications 3: 1103.

(a)

η_m (%)	Fl	Cy3	Cy3.5	A610	Cy5	Cy5.5	A700
2	71.9	28.1	-	-	-	-	-
3	65.0	25.4	9.6	-	-	-	-
4	64.8	25.3	9.6	0.3	-	-	-
5	64.6	25.2	9.5	0.3	0.4	-	-
6	64.1	25.0	9.5	0.3	0.4	0.7	-
7	62.2	24.2	9.2	0.3	0.4	0.7	3.0

(b)

	Fl-Cy3	Cy3-Cy3.5	Cy3.5-A610	A610-Cy5	Cy5-Cy5.5	Cy5.5-A700
r (Å)	32	21	19	34	21	36

(c)

R/R_0	F1	Cy3	Cy3.5	A610	Cy5	Cy5.5	A700
F1	0	0.47	0.80	1.28	--	--	--
Cy3	--	0	0.39	0.69	1.36	--	--
Cy3.5	--	--	0	0.32	0.88	1.34	--
A610	--	--	--	0	0.41	0.66	1.13
Cy5	--	--	--	--	0	0.31	0.82
Cy5.5	--	--	--	--	--	0	0.53
A700	--	--	--	--	--	--	0

Yellow: Nearest neighbor distances
Green: Next nearest neighbor distances

Table SIII. (a) The direct excitation levels for each of the dyes in structures with progressively increasing numbers of dyes present. (b) Estimates of the dye attachment point distances between the dyes as computed using the cylinder approximation. (c) The dye attachment point distances scaled by R_0 and highlighting the nearest neighbor and next-nearest-neighbor values.

	F1	Cy3	Cy3.5	A610	Cy5	Cy5.5	A700
$R_{k,k+1}$	52	36	38	34	41	60	--
ΔR	20	15	19	0	20	25	
$\Psi Q_i/\Psi_{scal}$	1.05	0.35	0.27	0.58	0.23	0.15	0.18
α_i	1.15	0.65	0.52	0.013	0.88	0.93	0.98

Table SIV. The nearest-neighbor dye spacings, quantum yields, and dye yields as determined by a least-square regression process described in the text.

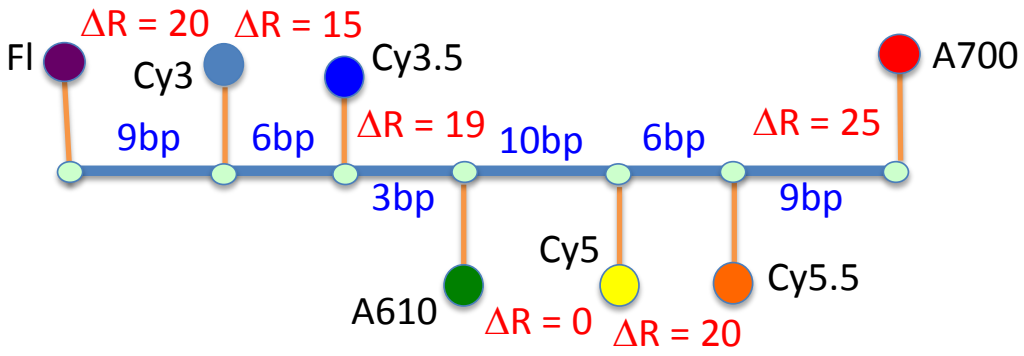

Fig. S3. Schematic depicting parameters given in Table SIV. Note that this schematic attempts to account for the underlying DNA helical structure in dye placements.

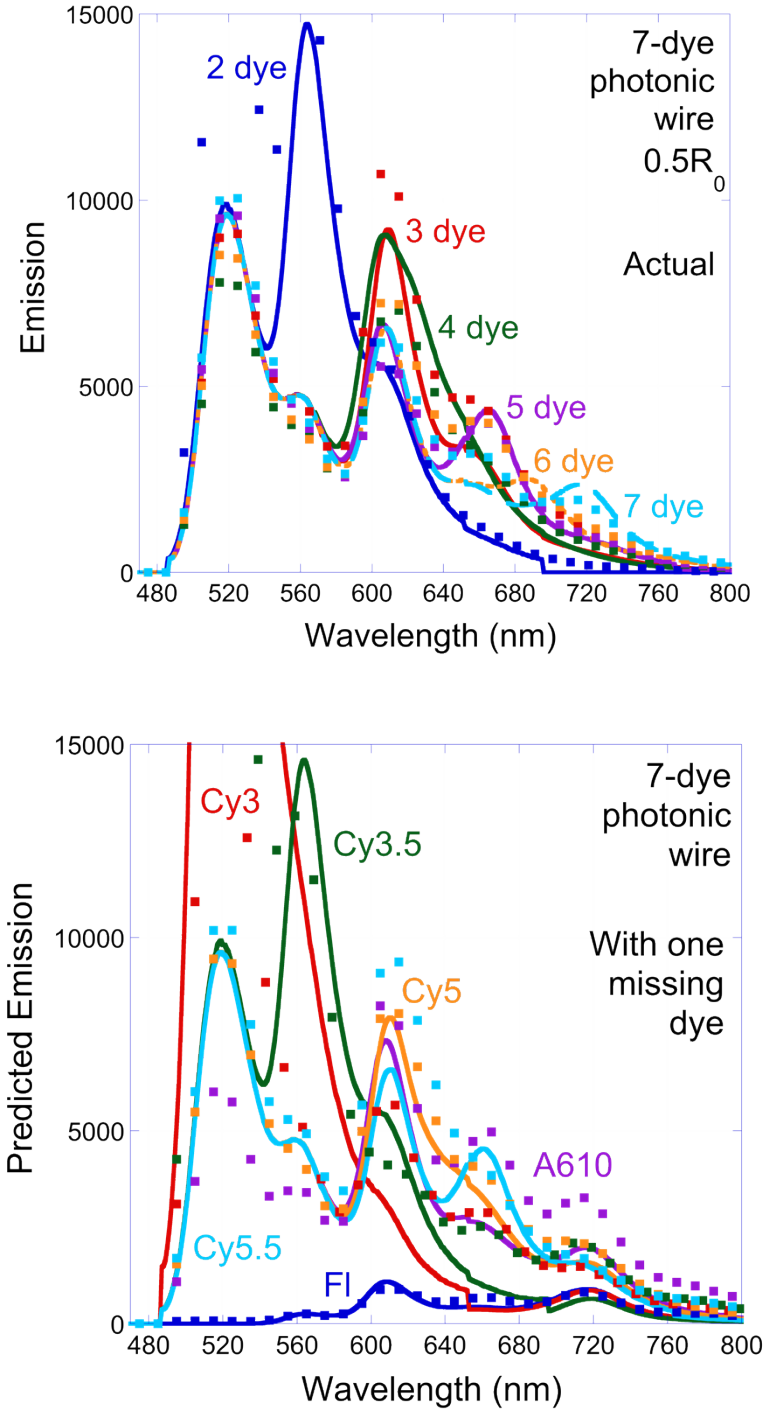

Fig. S4. Comparison between experimental spectra and simulated predictions for extend photonic wires with all dyes present (top) and with one missing as indicated for each curve (bottom).

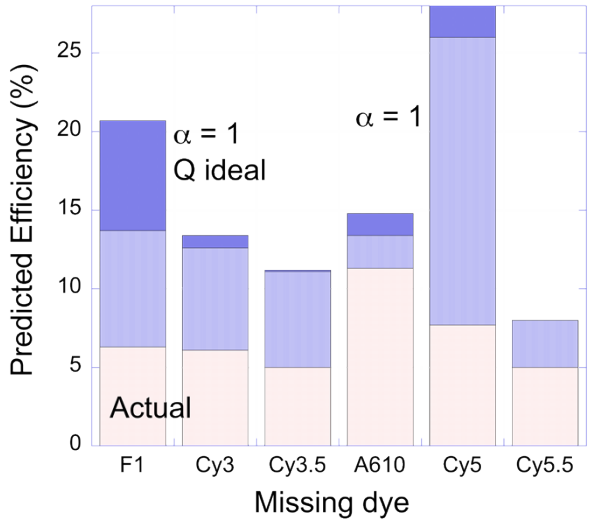

Fig. S5. Plots of the predicted anywhere-to-end efficiencies in the missing-dye experiments. Values for both "actual" and "ideal" cases are shown.

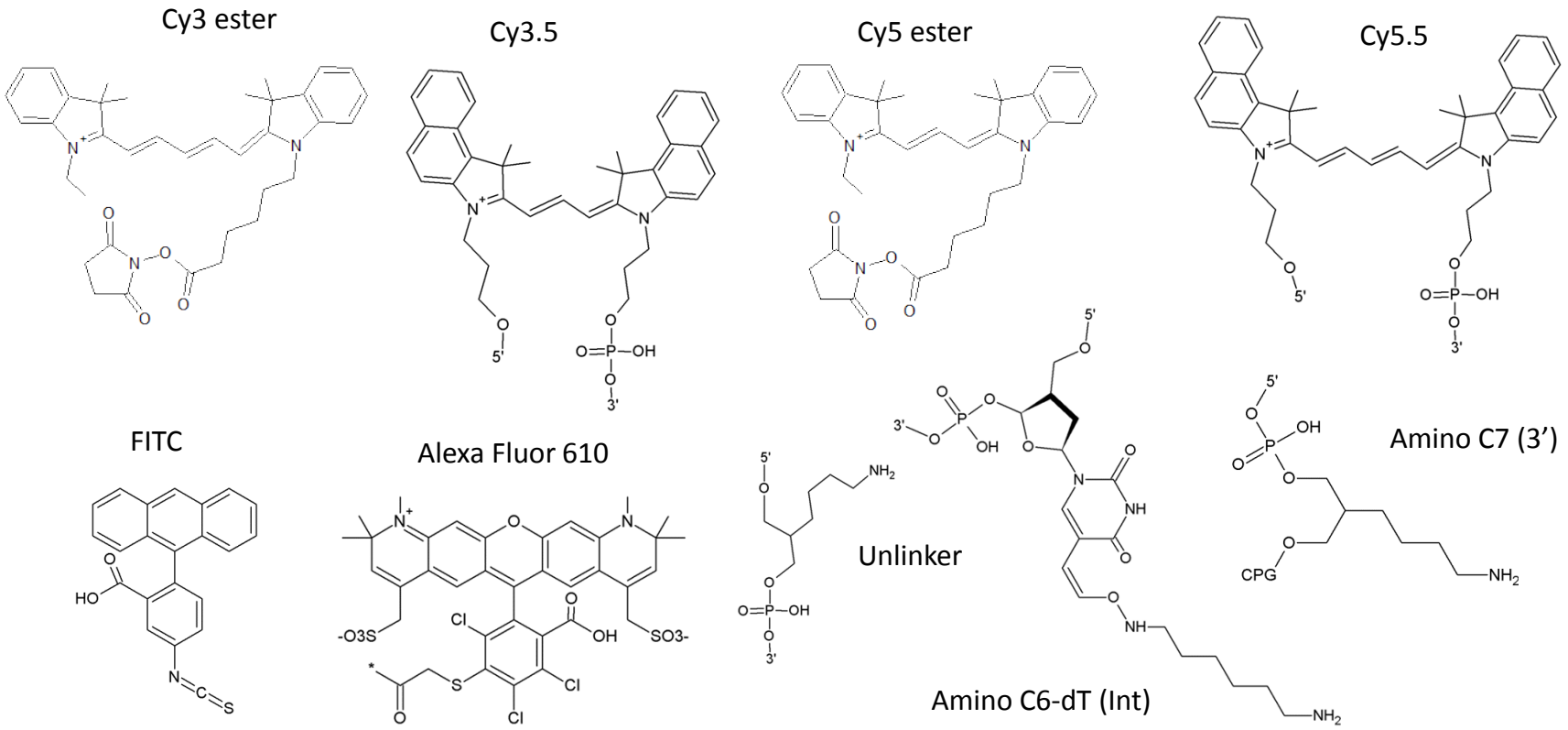

Figure S6. Chemical structures of the pertinent dyes used in this study along with DNA modifiers/linkers used to attach them to DNA. The Cyanine dyes are shown either following phosphoramidite insertion into the DNA sequence or as the original succinimidyl ester that is attached to an amino modifier. Fluorescein is shown as an isothiocyanate (FITC) for labelling amines. Alexa Fluor 700 structure is not shown as it is proprietary.

Table SVII. DNA Sequences

Name	Sequence 5'-3'	bps	Modification	Tm (1X/ 2.5X PBS)	Source
A	*TAATAGCTAATTCTA	15	5' Pacific Blue	39.5/ 44.9	Biosyn
B	TAGAATTAGCTATTACTCCT*CGTATC	26	Internal C6-Am dT - Fluorescein	59.9/ 65.4	Biosyn
C	CCT*GGACTAACATGCCGAGCTAGTGGT	27	Internal C6-Am dT - Cy3	71.5/ 76.4	Biosyn
D	*TAGTCCAGGGATACGAGGAG	20	5'Cy3.5	62.7/ 67.4	Biosyn
E	TCGGCAT*GT	10	Internal C6-Am dT – Alexa Fluor 610	38.4/ 42.4	Biosyn
F	ACGACCCAGACCACT*AGC	18	Internal C6-Am dT-Cy5	64.5/68.9	Biosyn
G	*CTGGGTCGTATCGCTTCCAATAGATTAAAATTA	33	5' Cy5.5	63.9/69.6	Biosyn
H	GGAAGCGAT*	9	3'Am C6 - Alexa Fluor 700	35.0/38.9	Biosyn
I	TAATTTTAATCTATT*	15	3' Am C6 - Alexa Fluor 750	34.9/40.7	Biosyn

*In sequence indicates modifier/dye placement. For Cy3.5 – Alexa Fluor 610 placement, the designed distance/separation was based on the cylinder model in which we assume the DNA is perpendicular to the axis and therefore the angular difference plus the linker length pushes the two dyes the appropriate distance away.

Table SVIII. Pertinent photophysical and FRET properties of the fluorophores used

Fluorophore	QY[1]	Ext. coeff. ($M^{-1}cm^{-1}$)	λ_{max} absorption	λ_{max} emission	$^2R_0$ in Å / $J(\lambda)$ in $cm^3\,M^{-1}$						
					Fl	Cy3	Cy3.5	AF610	Cy5	Cy5.5	AF700
Fluorescein	0.81	68,000	490 nm	513 nm	**50/1.06e^{-13}**	**68/6.47e^{-13}**	**66/5.51e^{-13}**	**56/2.05e^{-13}**	**58/2.43e^{-13}**	**53/1.41e^{-13}**	**52/1.26e^{-13}**
Cy3	0.27	150,000	552 nm	565 nm		**50/3.15e^{-13}**	**58/7.56e^{-13}**	**57/6.47e^{-13}**	**60/9.20e^{-13}**	**59/8.58e^{-13}**	**55/5.78e^{-13}**
Cy3.5	0.29	150,000	579 nm	597 nm			**48/2.12e^{-13}**	**59/8.10e^{-13}**	**67/1.66e^{-12}**	**66/1.47e^{-13}**	**63/1.20e^{-12}**
Alexa Fluor 610	0.83	132,000	608 nm	630 nm				**67/5.85e^{-13}**	**83/2.17e^{-12}**	**83/2.08e^{-12}**	**80/1.70e^{-13}**
Cy5	0.23	250,000	648 nm	667 nm					**63/1.44e^{-12}**	**71/2.93e^{-12}**	**69/2.44e^{-12}**
Cy5.5	0.20	250,000	678 nm	696 nm						**65/1.97e^{-12}**	**67/2.44e^{-12}**
Alexa Fluor 700	0.21	196,000	697 nm	718 nm							**66/2.05e^{-12}**

[1]Measured from dye-labelled DNA.
[2]R_0 and $J(\lambda)$ values are averages calculated from the spectra of all dye-labeled DNA used in this study.

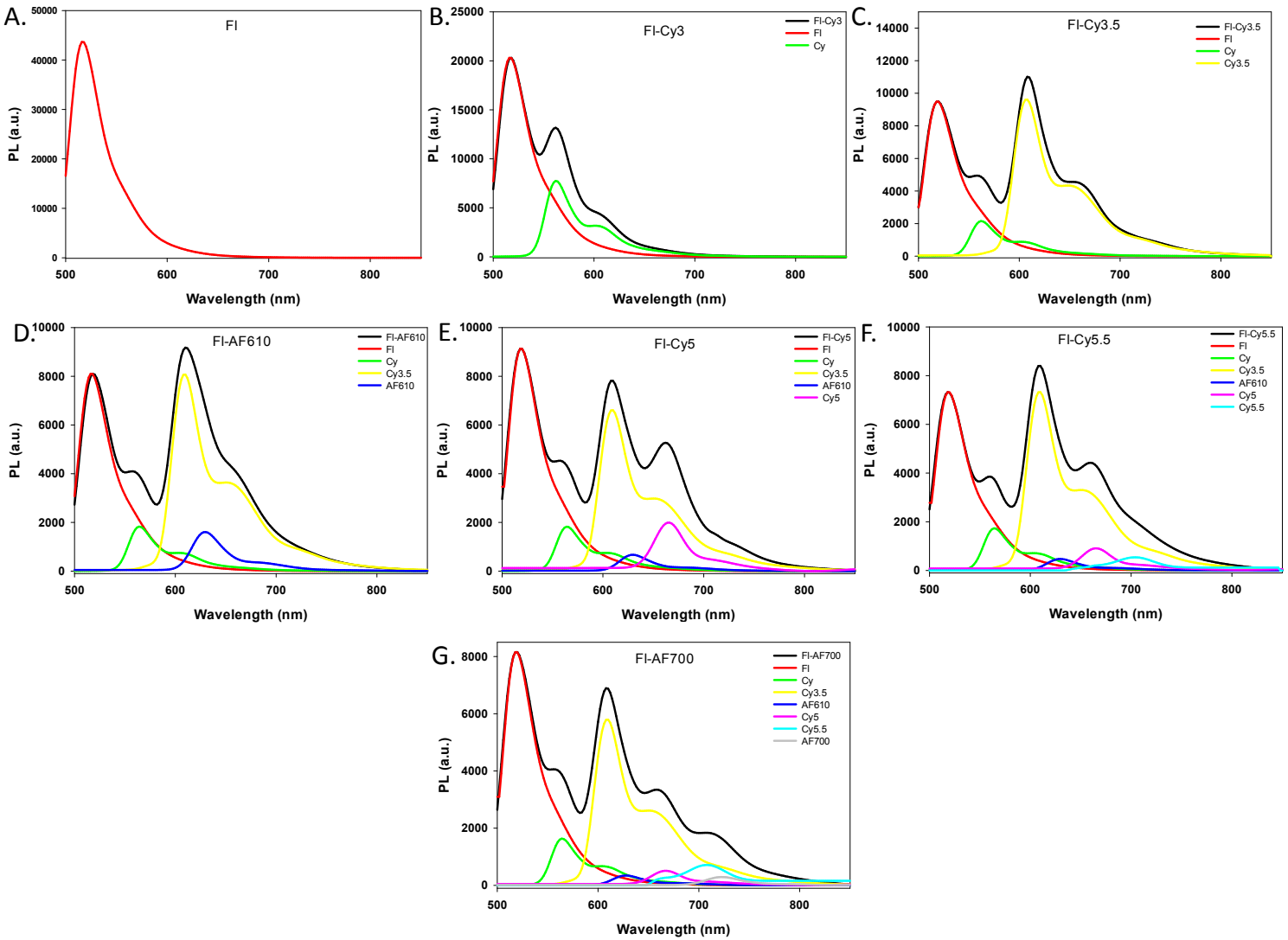

Figure S7. Experimental and deconvolved data for structures assembled with initial Fl dye and then sequential acceptors until the full Fl-AF700 construct is reached. This highlights the progressive evolution of the FRET response monitored in these systems.